ADVANCED MATERIALS INTERFACES
Open Access
www.advmatinterfaces.de

Check for updates

Surface Properties of p-GaN and Formation of Nickel Metal Contacts

Mikko Miettinen, Vesa Nuutila, Zahra Jahanshah Rad, Masoud Ebrahimzadeh, Anni Ruokonen, Risto Punkkinen, Juha-Pekka Lehtiö, Marko Punkkinen, Pekka Laukkanen, Kalevi Kokko, Sami Suihkonen, Hele Savin, and Weimin Wang*

Nickel (Ni) is the key component in ohmic contacts for Mg-doped p-GaN, but the detailed formation mechanisms of the ohmic contact have not yet been understood. In this work, the effect of potassium hydroxide (KOH)-based chemical treatment on the surface of p-GaN is investigated using X-ray photoelectron spectroscopy (XPS), scanning tunneling microscopy (STM), and low-energy electron diffraction (LEED). Ni metal contacts on the chemically treated p-GaN surface are studied using transfer length method (TLM) and synchrotron radiation photoelectron spectroscopy (SR-XPS). The chemical treatment of p-GaN improves the brightness of the (1x1) hexagonal diffraction pattern in LEED and keeps the 2D terrace structure in STM visible. Concomitantly, XPS shows that the amount of O, C, and Mg–O bonds at the surface were reduced. Ni/p-GaN provided an ohmic contact after annealing in ultra-high vacuum (UHV) at 500 °C. Simultaneously, SR-XPS shows the diffusion of Ga to Ni and the formation of a previously unreported Ga 3d component, which has a surprisingly narrow line shape, indicating that it originates from a crystalline interface phase. Diffusion of Ga is discussed to cause Ga vacancies and acceptor levels in the bandgap increasing carrier tunneling, thus enabling ohmic contact.

1. Introduction

Manufacturing low-resistive ohmic contacts is crucial in order to reduce the resistive heating losses in semiconductor devices. The efficient p-type doping of GaN by Mg ions and high-quality contacts on p-GaN have been an exceptional challenge, but great achievements (e.g., refs. [1, 2]) have enabled the development of GaN-based technology. The main reasons causing issues in ohmic contact formation are the high Schottky barrier, the high ionization energy of the Mg acceptors, and the Mg-H complexes.[3]

Fermi-level pinning has been observed for both n- and p-GaN. At the same time, the Schottky barrier is clearly higher for p-GaN than for n-GaN with multiple metals: although the metal/n-GaN contact can have a Schottky barrier of 1 eV, the metal/p-GaN contact barrier height can be over 2 eV. The difficulty in finding a suitable metal for the low Schottky barrier contact for p-GaN is due to the high work function requirement for the metal. On the other hand, even if the metal work function would be higher than p-GaN, resulted barrier height most likely doesn't follow the standard Schottky-Mott behaviour.[4,5]

One of the most typical ways to make ohmic contact formation easier is to increase the dopant concentration, which makes the tunnelling through a probable Schottky barrier possible. However, from the beginning of Mg doping to create p-GaN, the concentration of Mg atoms and the actual effective hole concentration have been very different. Despite Mg concentrations exceeding even 10^{20} cm^{-3}, the effective hole concentration can be in range of 10^{16} cm^{-3} after dopant activation.[1] One issue is the presence of hydrogen during the dopant activation, which leads to Mg-H complex formation at temperatures over 400 °C. Furthermore, different Mg acceptor states have been found to form.[6] Complex formation leads to hole compensation, thus significantly increasing the resistivity of the material and decreasing the effective doping concentration.[2] At the same time, simply increasing the dopant concentration only works to a certain extent.[7]

M. Miettinen, V. Nuutila, Z. Jahanshah Rad, M. Ebrahimzadeh, A. Ruokonen, R. Punkkinen, J.-P. Lehtiö, M. Punkkinen, P. Laukkanen, K. Kokko
Department of Physics and Astronomy
University of Turku
Turku FI-20014, Finland
E-mail: miolmi@utu.fi

S. Suihkonen, H. Savin
Department of Electronics and Nanoengineering
Aalto University
Espoo FI-02150, Finland

W. Wang
MAX IV Laboratory
Lund University
PO Box 118, Lund SE-22100, Sweden

The ORCID identification number(s) for the author(s) of this article can be found under https://doi.org/10.1002/admi.202500163

© 2025 The Author(s). Advanced Materials Interfaces published by Wiley-VCH GmbH. This is an open access article under the terms of the Creative Commons Attribution License, which permits use, distribution and reproduction in any medium, provided the original work is properly cited.

DOI: 10.1002/admi.202500163

21967350, 2025, 13, Downloaded from https://advanced.onlinelibrary.wiley.com/doi/10.1002/admi.202500163 by Duodecim Medical Publications Ltd, Wiley Online Library on [27/08/2025]. See the Terms and Conditions (https://onlinelibrary.wiley.com/terms-and-conditions) on Wiley Online Library for rules of use; OA articles are governed by the applicable Creative Commons License

Table 1. Layer thicknesses and doping concentrations of the samples.

Sample	d_{GaN} [μm]	$d_{p\text{-}GaN}$ [μm]	$p_{p\text{-}GaN}$ [1/cm^3]	$d_{p^+\text{-}GaN}$ [nm]	$p_{p^+\text{-}GaN}$ [1/cm^3]
Electrical measurement (M3 808)	1.8	1	$6 \cdot 10^{16}$	20	$1 \cdot 10^{18}$
Synchrotron 1 (M3 A19)	2.3	1.05	$2 \cdot 10^{15}$	10	$1 \cdot 10^{18}$
Synchrotron 2 (M2 1732)	3	0.8	$4 \cdot 10^{16}$	10	$2 \cdot 10^{17}$

Despite these problems, an annealed metal stack of Ni covered with Au or Pt is used to make ohmic contacts on p-GaN. Previously, Ni/Au configuration has proven to be a good contact composition with clear, multiple orders of magnitude difference in contact resistivity compared to Ni/Pt (4×10^{-6} Ωcm^2 vs 2.5×10^{-2} Ωcm^2, respectively).[8] The stack requires heating in order to form a good ohmic contact and typically a temperature from 500 °C upwards. Some different metal stacks can require even temperatures as high as 750 °C.[9] The annealing background can be either inert gas or oxidizing ambient, however the oxidizing ambient provides lower contact resistivity.[10] Two important reactions occur during annealing Ni/Au in O_2: the metal layers invert so that the Ni diffuses to the surface making Au to be in direct contact with the p-GaN, and Ni oxidizes to NiO. When using an inert background, there is no such clear metal layer inversion. Some diffusion of Ni to the Au layer does occur, leading to the formation of Au-Ni alloy, but the Au layer stays on top and does not diffuse to the p-GaN surface as it does with O_2 annealing.[8,10,11] The high solubility of Ga to Au has been proposed to also be one reason for the decreased contact resistivity, as intermixing of Ga and Au would cause beneficial Ga vacancies.[12] Gallium vacancies have also been seen to form with Pd/Ni/Au contact structures where Ga-Pd alloy is formed as a result of annealing, providing low contact resistivity.[13]

On the other hand, in order to integrate p-GaN complementary metal-oxide-semiconductor (CMOS) technology to Si CMOS processing lines, Au free contacts have to be developed to avoid possible Si CMOS process line contamination due to strong diffusion of Au. A stack of Mg/Ni/Pt has recently been investigated, and Ni seems to also play an important role in the creation of Ga vacancies, leading to decreased contact resistivity. Interestingly, in this case the oxygen ambient during annealing was noticed to result a Schottky contact.[14]

In this work, we study a simplified system with pure Ni on the p-GaN surface to clarify the role of Ga-Ni interaction in the ohmic contact formation. We demonstrate that this contact process is associated with the formation of a crystalline $GaNi_x$ alloy which causes an unusually sharp Ga 3d core-level shift seen in X-ray photoelectron spectroscopy (XPS). We conclude that as-deposited Ni contacts are Schottky type, but post-annealing in ultra-high vacuum (UHV) leads to ohmic behaviour due to NiO enhanced Ga diffusion, creating Ga-vacancy mediated gap levels providing enhanced tunneling through the Schottky barrier.

2. Experimental Methods

2.1. Sample Preparation

GaN films were deposited using Metal Organic Vapor Phase Epitaxy (MOVPE) with two different reactors, M2 and M3, on sapphire substrates. Films consisted of sapphire/GaN/p-GaN/p$^+$-GaN layer stack with varying GaN layer thicknesses d and doping concentrations p. All samples were doped with Mg. The specifications of each sample are shown in **Table 1**.

GaN surfaces were treated by immersing the samples in 4 m potassium hydroxide (KOH) solution at 60 oC for 1 min, followed by a 1 min immersion in deionized water (DIW). After treatment, a layer of nickel was deposited on the sample surface using Bal-Tec Med 020 sputtering device. The device was in a separate location, and due to that, the samples were exposed to air for 20 minutes. The metal film thicknesses for the electrical measurement samples and synchrotron samples were 100 and 3 nm, respectively. The contacts for electrical measurements were patterned with standard lithography using a positive photoresist. The excess metal was etched using room temperature hydrochloric acid (HCl) (37 %):DIW (1:2) solution. The final contact pattern consisted of rectangular contacts with dimensions of KOH solution at 60 °C for 1 min, followed by a 1 min immersion in deionized water (DIW). After treatment, a layer of nickel was deposited on the sample surface using Bal-Tec Med 020 sputtering device. The device was in a separate location, and due to that, the samples were exposed to air for 20 minutes. The metal film thicknesses for the electrical measurement samples and synchrotron samples were 100 and 3 nm, respectively. The contacts for electrical measurements were patterned with standard lithography using a positive photoresist. The excess metal was etched using room temperature HCl (37 %):DIW (1:2) solution. The final contact pattern consisted of rectangular contacts with dimensions of 300 μm x 600 μm (width x length) in four rows A–D. In each row, the first distance between the contacts was 300 μm, and the distance increased by 100 μm after each contact (that is, distance A1–A2 was 300 μm, A2–A3 400 μm etc.). For surface characterisation experiments without metal contacts/layer the loading time from KOH solution to vacuum was 5 min.

The metal-contact samples were post-heated using UHV multi-chamber consisting of load lock, preparation chamber and analysis chamber. The heating was executed using resistive heating, i.e., conducting current through a heater element made of tungsten wire beneath the sample in the analysis chamber. The base pressure of the chamber was below 10^{-9} mbar. Sample temperature was observed using a pyrometer with emissivity of 0.63 by measuring through a vacuum chamber viewport.

2.2. Surface and Electrical Characterization

Scanning tunnelin microscopy (STM, low-energy electron diffraction (LEED), XPS, and synchrotron radiation XPS (SR-XPS) were used for surface characterization. STM and LEED

 © 2025 The Author(s). Advanced Materials Interfaces published by Wiley-VCH GmbH

21967350, 2025, 13, Downloaded from https://advanced.onlinelibrary.wiley.com/doi/10.1002/admi.202500163 by Duodecim Medical Publications Ltd, Wiley Online Library on [27/08/2025]. See the Terms and Conditions (https://onlinelibrary.wiley.com/terms-and-conditions) on Wiley Online Library for rules of use; OA articles are governed by the applicable Creative Commons License

were located in the same UHV multi-chamber where the heating was performed. XPS used a monochromated Al K-α x-ray source with charge compensation. The spot size used was 200-300 µm depending on the measurement. Synchrotron radiation XPS measurements were performed at the solid-state end station (SSES) of the FinEstBeaMS beam line in the MAX IV Laboratory.[15,16] For contact resistivity characterization a transfer length method (TLM) was used.[17] Measurements were performed with Rucker & Kolls 666 4-point probe needle probing stage connected to the HP4145B semiconductor parameter analyzer driven by a LabView program. The measuring voltage range used was from –200 to 200 mV.

3. Results and Discussion

3.1. Surface of Chemically Treated GaN

Prior to surface treatment, the GaN surface had a clear LEED diffraction pattern despite the native oxide, as seen from **Figure 1A**. It is interesting that the GaN surface gives a diffraction pattern even with native oxide, suggesting that it accommodates oxygen atoms in an unusual manner in the crystalline structure. Typically, no LEED pattern is observed from a native oxide covered semiconductor surface. However, the observation is consistent with the previous results.[18] STM images in Figure 1B show that before KOH treatment the surface has a clear terrace structure, but the zoomed-in image shows white dots on the surface. The amount of these dots is reduced after the KOH treatment. Based on the changes seen in the XPS in **Figure 2**, the white dots are associated with MgO: the amount of oxygen decreases at the surface, and at the same time the peak shape of Mg 1s clearly changes to be more metallic component dominant. The line shape before and after KOH is also affected by Ga 2s peak, which has a binding energy of 1301 eV at metallic form.[19] At the same time, there's no such observable change in Ga 3d spectrum (spectra not shown). Therefore, we expect that no change is happening to 2s peak, and thus changes in Ga bonding would not explain these changes. The surface still clearly has oxygen on it, which was expected since the KOH treated sample was transferred to the measurement system via air, resulting it to be exposed to contaminants in the air. Due to the clear amount of oxygen, we also can't rule out the possibility of some gallium oxide on the surface.

We know from the p-GaN growth process that the amount of Mg on the surface is higher than the effective hole concentration - not all Mg is actively contributing to the hole concentration. Thus, we expect that the Mg bonded with O isn't contributing to doping, and thus the decrease of MgO at the surface doesn't change the doping concentration at the surface. Indeed, Mg atoms have been previously found to occupy different crystal states and cause different acceptor states.[6,20]

Figure 1C shows scanning tunneling spectroscopy (STS) curves from the surface before and after KOH treatment. The treatment had changed the Fermi level position by approximately 0.5 eV closer to the valence band maximum. This is in line with findings presented in the literature.[22] Such change is beneficial for contact formation, as it lowers the surface barrier height which is one of the key issues in contact fabrication for p-GaN. A drop in the conduction band around 3 V can be a result of local Ga oxide affecting the conduction at the surface. However, it's worth noting that the Fermi level position was measured in UHV without any metal, and might change as a result of metal layer deposition.

3.2. Electrical Results

Once the metal contacts were deposited, the first round of electrical measurements were done (**Figure 3A**). Without any heating following metal deposition, the contact was Schottky type. Also, as the distance between the measured metal contacts increases, the measured currents should drop accordingly, i.e., the maximum current measured between contacts B2 and B3 should be higher than the one measured between B3 and B4, which again should be higher than measured between B4 and B5. However, this doesn't hold with unheated contacts: from B3 to B4 the maximum currents measured on both end of voltage range were higher than that of from B2 to B3. Overall, while the contacts were measurable, they didn't give consistent TLM results.

Contacts were post-annealed in UHV chamber at 500 °C for 5 min. The base pressure during the heating was 10^{-8} mbar. Now the IV characteristics had turned to ohmic type (Figure 3B), and the amount of current flowing had increased by an order of magnitude. The current decreased as the contact distance increased, as it should. Resulted curves followed the TLM theory, and we were now able to extract contact resistivity. There, however, was still some inconsistency in the results: resistivity was determined using two different contact rows, and both of these rows provided different contact resistivities. B and C contact rows provided 6.50 Ωcm^2 and 10.46 Ωcm^2, respectively. Due to this, we decided to experiment with a background gas.

The Second sample was prepared in the same way as the first one. Before post-metallization anneal, the IV curve was similar to the first sample, with Schottky type contacts. Annealing was done in same UHV chamber, which was used earlier, but this time NH_3 gas was introduced to the chamber. The partial pressure of NH_3 in the chamber during heating was 5×10^{-6} mbar, while other heating parameters were the same. As Figure 3C shows, the resulting contacts were also ohmic, but the currents were higher compared to the plain UHV anneal. The contact resistivity achieved was 5.45 Ωcm^2 and 5.65 Ωcm^2 from the rows B and C, respectively. The results are now more consistent, and the resistivity has decreased.

The difference between the effects of the oxygen background and other gases can be significant: if the Ni/Au stack is annealed in Ar at 500 °C, the contact resistivity is in the same order of magnitude as we achieved in UHV with less than twice as large doping concentration.[23] Based on this, the reason why heating in plain UHV doesn't provide low contact resistivity is the nonreactivity of the interface elements and the environment, suggesting a need of an oxidizing environment.

The obtained contact resistivities are no nowhere near the lowest reported ones (e.g.,[3] but obtaining such values was not our goal in this study. Several parameters affect the final contact resistivity: surface cleanliness, atomic level smoothness,

© 2025 The Author(s). Advanced Materials Interfaces published by Wiley-VCH GmbH

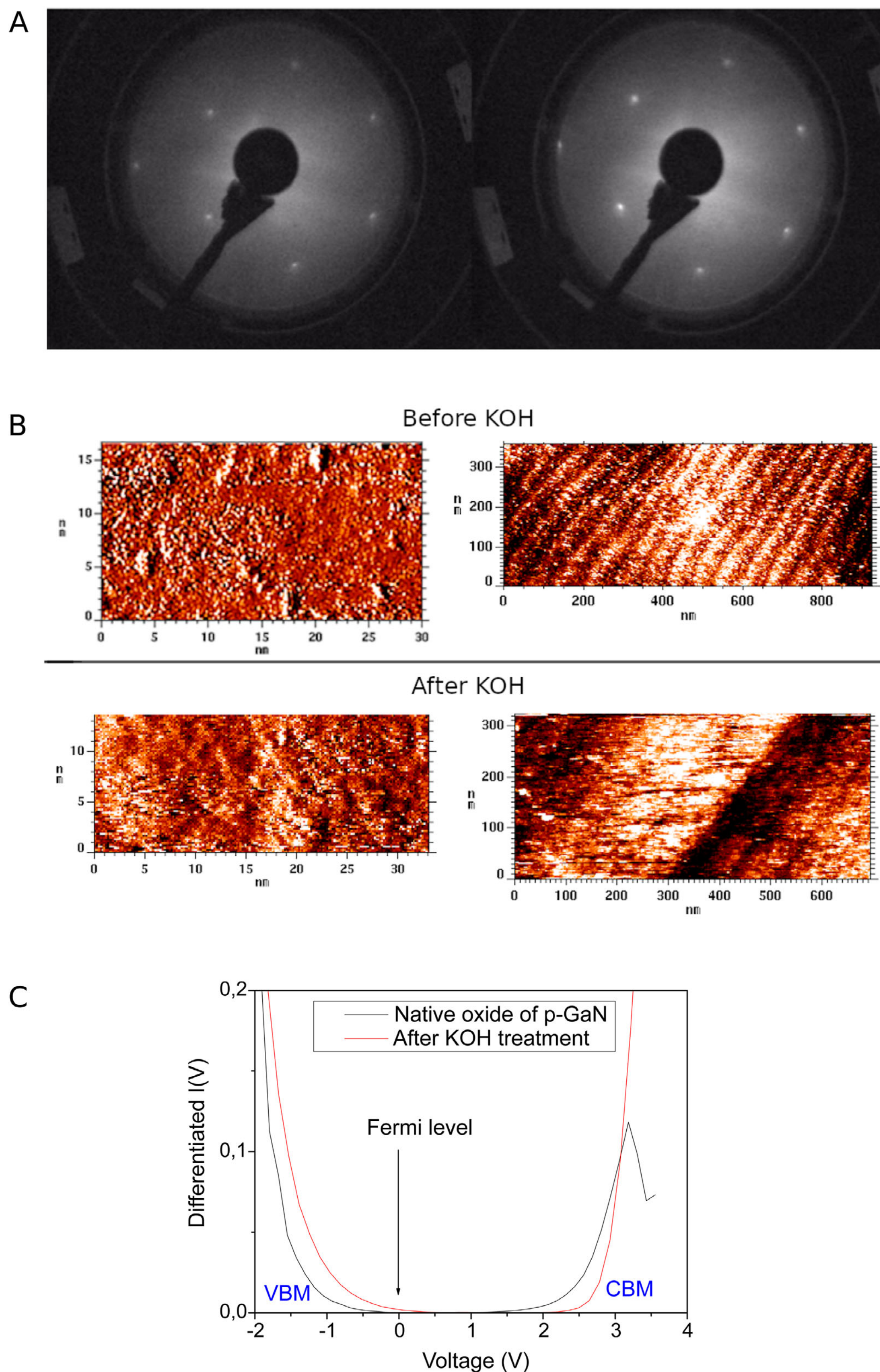

Figure 1. A) LEED image showing hexagonal (1x1) pattern before (left) and after (right) KOH treatment. Surface measured with 203 eV electron energy. B) STM images before and after KOH treatments. White dots visible in zoomed-in image measured before KOH treatment disappear due to the treatment. C) STS curves showing that the position of Fermi level changes toward valence band maximum (VBM) as a result of KOH treatment. Part of LEED and STM figures are reproduced under terms of the CC-BY license[21] Copyright 2024, Institute of Physics.

 © 2025 The Author(s). Advanced Materials Interfaces published by Wiley-VCH GmbH

21967350, 2025, 13, Downloaded from https://advanced.onlinelibrary.wiley.com/doi/10.1002/admi.202500163 by Duodecim Medical Publications Ltd, Wiley Online Library on [27/08/2025]. See the Terms and Conditions (https://onlinelibrary.wiley.com/terms-and-conditions) on Wiley Online Library for rules of use; OA articles are governed by the applicable Creative Commons License

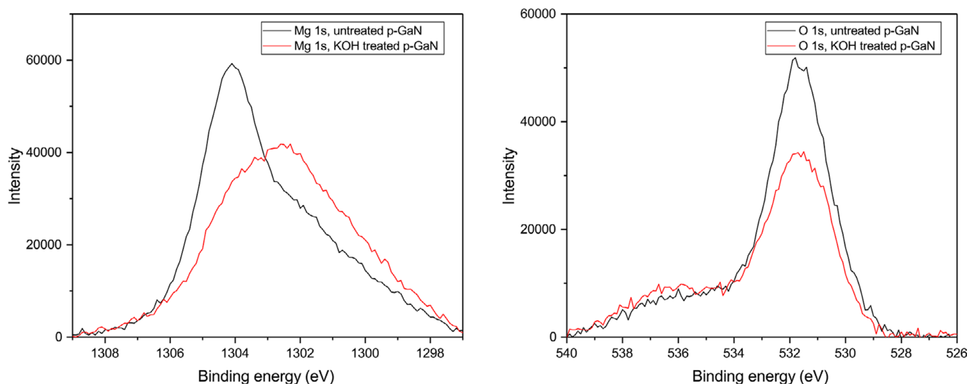

Figure 2. O 1s and Mg 1s XPS spectra from GaN surface before and after KOH treatment. O 1s spectra shows a clear decrease in oxygen concentration even though there's no change in the Ga 3d spectra.

post-heating temperature and environment as well as surface doping concentration.[8,12,24,25] We wanted to investigate whether it is possible to switch Schottky contacts to ohmic type with Ni, and if so, what happens to the chemical composition at the interface concomitantly. For chemical composition investigation, we utilized synchrotron radiation XPS.

3.3. Synchrotron XPS Measurements

For synchrotron measurements two identical samples were made. Both samples had the wet chemically treated p-GaN with 3 nm of nickel on top. No post-metallization treatments were done before synchrotron measurements. Since oxidation of Ni was

Figure 3. *I–V* curves of contacts measured from contact row B. A: before UHV annealing, B: after UHV annealing, C: after NH_3 background annealing, and D: all situations plotted in logarithmic scale. The number in the legend represents the contact number on the row.

© 2025 The Author(s). Advanced Materials Interfaces published by Wiley-VCH GmbH

21967350, 2025, 13, Downloaded from https://advanced.onlinelibrary.wiley.com/doi/10.1002/admi.202500163 by Duodecim Medical Publications Ltd, Wiley Online Library on [27/08/2025]. See the Terms and Conditions (https://onlinelibrary.wiley.com/terms-and-conditions) on Wiley Online Library for rules of use; OA articles are governed by the applicable Creative Commons License

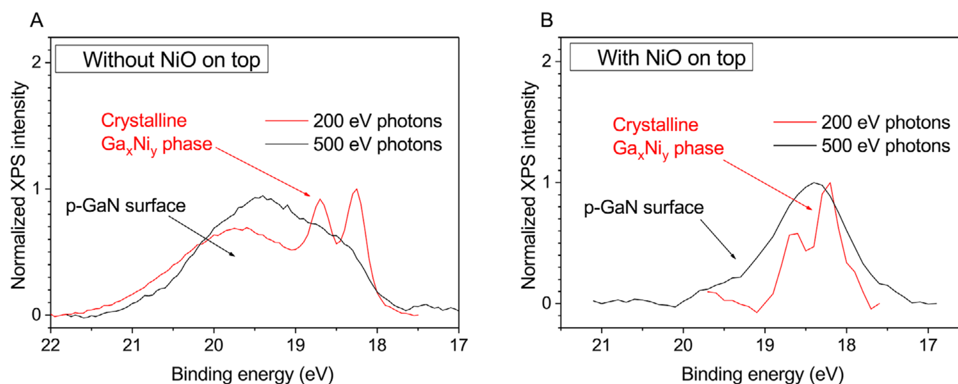

Figure 4. Synchrotron spectra of Ga 3d measured with 200 eV and 500 eV photons after heating from A: sample without NiO on the surface B: with NiO on the surface.

expected, separate sample with similar metal layer was measured with *ex-situ* Al K-α XPS using depth profiling to make sure that the 3 nm layer wasn't oxidized through. Gentle Ar ion cluster sputtering proved that just the top layer of Ni, 1.6 nm at maximum, was oxidized after 13 days of air exposure. The oxide thickness was estimated using the Beer–Lambert law.

FinEstBeaMS solid-state end station provided a possibility for heating and argon sputtering. In order to study the changes in the interface composition at different depths, two different approaches were taken: first sample was heated without any sputtering at 500 °C for 5 min, while with the second sample the Ni layer was sputtered so that the Ga 3d signal from p-GaN was detectable, and then heated with similar parameters as the first sample. For clarity, sample heated without sputtering is marked as sample with NiO, and sample that was first sputtered and then heated as sample without NiO. Different photon energies were utilized to study material compositions in different depths in the samples.

Figure 4 shows results of heating from both samples, measured with very surface sensitive photons with 200 eV energy and a bit deeper penetrating photons with 500 eV energy. Heating has clearly caused gallium diffusion toward the top surface, as can be seen from sample heated with NiO. Prior to heating, no gallium was observed even with high photon energies up to 1100 eV. After heating, a clear spin-orbit splitted Ga 3d component, which is shifted 1.4 eV to lower binding energy from Ga 3d component of p-GaN, appears in the 200 eV spectrum. Peaks are sharp, implying crystallinity from atomic origin, and since this wasn't observable before heating, gallium must have diffused to the nickel layer. At the same time, no oxygen was detected after the heating (not shown), implying that the NiO layer has been removed during the UHV heating. 500 eV photon measurement covers same binding energy region with slightly wider tail at the higher binding energy end, coming from the substrate surface. This tail is most likely arising from Ga–O bonds at the surface, as discussed earlier regarding STS results.

For the sample heated without NiO, the signal from the p-GaN substrate is clearly visible with both 200 eV and 500 eV as a wide component at higher binding energies. This is no surprise, as the surface was sputtered until a clear Ga 3d signal from p-GaN was achieved already before heating. These spectra also show the formation of additional Ga 3d component: 200 eV spectrum shows clear 3d splitting, and 500 eV spectra clearly show a separate, yet indistinguishable component on the lower binding energy end, indicating metallic environment for atoms of this new component.

Based on the measurements from the KOH treated p-GaN surface, the starting surface consists of Ga–N and Ga–O bonds. Thus, the components at higher binding energies measured with SR-XPS should be composed of these same components. **Figure 5** shows how the chemically treated surface measured with Al K-α XPS compares to 200 eV measurement from sample heated without NiO. The wide component consisting of surface bonds of p-GaN substrate in the heated sample is clearly at higher binding energy than the same bonding environment signal observed with standard XPS, i.e., there's a clear binding energy shift. The width of the standard XPS peak compared to synchrotron XPS peak rises from multiple inseparable bonding environments, as well as much higher pass energy compared to synchrotron measurement (50 vs 1 eV, respectively).

As seen from **Figure 6**, some shifting in Ga 3d occurs already before heating compared to the chemically treated surface.

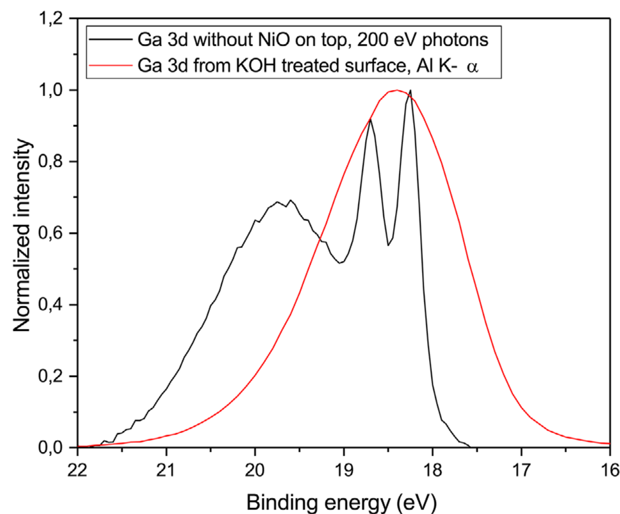

Figure 5. Comparison between 200 eV measurement made using synchrotron from sample heated without NiO on top (black) and measurement of KOH treated p-GaN without metal layer using Al K-α XPS (red).

© 2025 The Author(s). Advanced Materials Interfaces published by Wiley-VCH GmbH

21967350, 2025, 13, Downloaded from https://advanced.onlinelibrary.wiley.com/doi/10.1002/admi.202500163 by Duodecim Medical Publications Ltd, Wiley Online Library on [27/08/2025]. See the Terms and Conditions (https://onlinelibrary.wiley.com/terms-and-conditions) on Wiley Online Library for rules of use; OA articles are governed by the applicable Creative Commons License

21967350, 2025, 13, Downloaded from https://advanced.onlinelibrary.wiley.com/doi/10.1002/admi.202500163 by Duodecim Medical Publications Ltd, Wiley Online Library on [27/08/2025]. See the Terms and Conditions (https://onlinelibrary.wiley.com/terms-and-conditions) on Wiley Online Library for rules of use; OA articles are governed by the applicable Creative Commons License

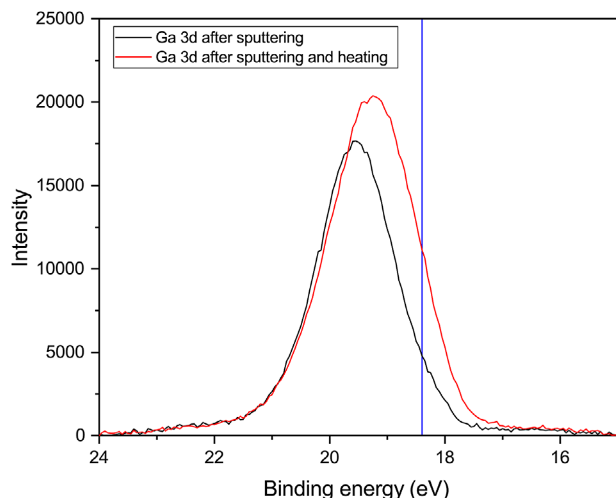

Figure 6. Ga 3d spectra before (black) and after (red) annealing. Both curves were measured after sputtering and show a clear shift toward higher binding energy compared to chemically treated surface (blue vertical line).

However, Ga–Ni interaction and alloying leading to a new Ga 3d component occurs during the post heating: comparing the curves before and after the heating shows that at higher binding energy end the curves follow same path, but after heating there's clearly a new component at lower binding energy area.

3.4. Mechanism of Contact Type Change

The shifting of the whole Ga spectrum toward a higher binding energy (Figure 5) is an implication of bands bending downwards because the binding energy separation to the Fermi level reference increases. Band alignment in Schottky contact for p-type semiconductor already causes the bands to bend downwards, which is then further increased due to heating. The depletion region width W has to increase a bit due to the increased barrier height for increased band bending. Since the bands bend downwards and the band structure is still Schottky-like but we see ohmic-like behavior in I–V curves, we conclude that the conduction mechanism at the interface is tunnelling. Thus, the depletion region can't widen much, otherwise carriers couldn't tunnel through the barrier.

On the other hand, even though the depletion region wouldn't increase much, carriers aren't able to tunnel before heating, so without additional changes at the band gap at the interface there can't be ohmic-like contact. As the gallium diffuses from the p-GaN toward the metal, it leaves Ga vacancies in the crystal structure. Gallium vacancies have previously been shown to act as acceptor states when there's no surface oxides present.[26] This most likely is the cause for ohmic-like behaviour in our contacts.

We propose a model in which the gallium diffusion induced vacancies generate extra electron levels which lie close to the valence band in the band gap. These levels act as a path for carriers to tunnel through the Schottky barrier, enabling ohmic-like behaviour as illustrated in **Figure 7**.

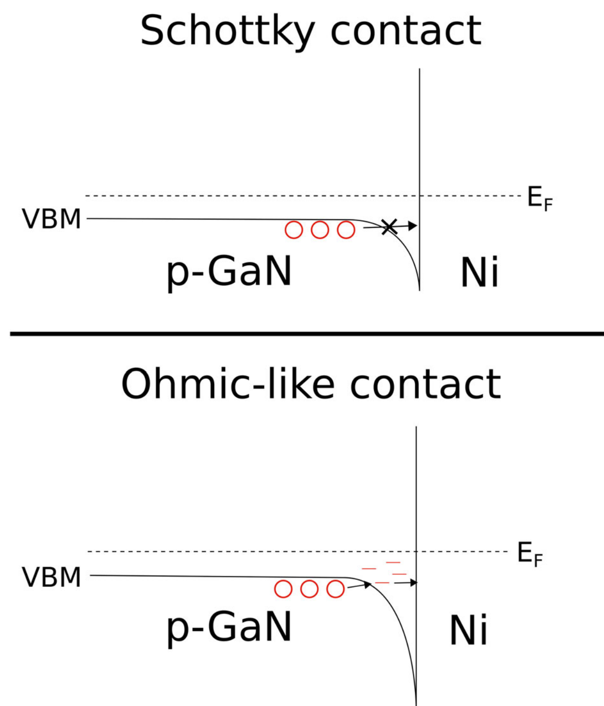

Figure 7. Illustrative schematic showing the change in the bands as a result of heating. In the Schottky contact the holes (red circles) can't pass the Schottky barrier. After heating, the Ga induced vacancies (red lines) lie in the depletion region, providing a path for the holes to tunnel through the barrier.

Diffused gallium is bonded with nickel in the interface, resulting in a crystalline GaNi phase. Previously, it has been shown that heating at 650 °C leads to formation of the $GaNi_3$ phase.[27] Although our annealing temperature is lower, more gallium dominant phases, i.e., GaNi and Ga_2Ni_3 are seen to form at a higher temperature of 800 °C, making the $GaNi_3$ more probable. The role of this bonding phase to contact resistivity in our contacts is unknown.

Moreover, we speculate that some nitrogen might be released from the interface due to the Ga diffusion. Nitrogen vacancies are known to provide a compensating n-type doping.[28,29] The SR-XPS also revealed several components for N 1s after annealing, indicating changes in nitrogen bonding environments as seen in **Figure 8**: The surface after sputtering only has Ga–N related N 1s component at 397.3 eV, and this resembles the situation at the interface before any heating. By heating the surface, two additional components appear, but the component ratios depend on whether the heating was done first or after the sputtering. When heating first, an additional component at 398.6 eV is the most dominant, while in the surface heated after sputtering the Ga–N related component is still most dominant, while also the additional component 398.6 eV is visible. These additional N 1s components most likely arise from nitrogen atoms which, have diffused toward the Ni metal surface, where they have formed different bonding structures with carbon. The source for carbon is most likely some contaminants in the Ni layer, which can come from the outgassing of the sample holder during the heating. When we used the NH_3 background during the metal contact post-heating, the resistivity lowered and became more uniform. NH_3 could have acted as a suppressing agent, reducing the formation of nitrogen vacancies.

 © 2025 The Author(s). Advanced Materials Interfaces published by Wiley-VCH GmbH

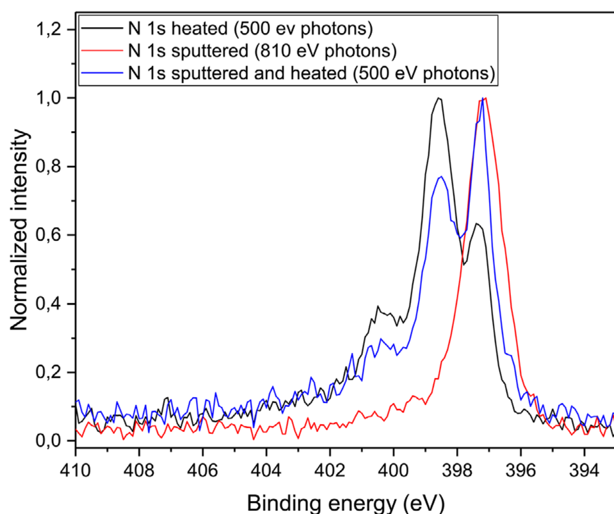

Figure 8. Synchrotron XPS spectra from heated (black line), sputtered (red line), and sputtered and heated (blue line) surfaces. In both heated spectra the surface composition has clearly changed in comparison to surface after sputtering, but the component ratios are different: heating the surface first resulted the pure N 1s component at 398.6 eV to be more dominant, as where as heating after sputtering kept the Ga–N related component at 397.3 eV to be more dominant.

4. Conclusion

We have investigated the effect of KOH wet chemical treatment and the Ni contact formation on p-type Mg-doped GaN. LEED and STM show that even without any chemical treatment a diffraction pattern and terrace structure can be seen, which is unusual for semiconductors. The KOH treatment also changes the Fermi level position toward valence band maximum. The oxygen concentration at the surface is decreased based on XPS results, and clear change in Mg 1s can be seen. This indicates that unactive Mg dopant atoms are bonded with O, and some Mg is removed during KOH treatment.

Without any heating, Ni forms Schottky contact with the KOH pre-treated p-GaN surface. Heating in UHV at 500 °C changed the contact type to ohmic, but the contact resistivity is far from the state-of-the-art resistivity. The resistivity wasn't uniform throughout the sample, but by heating in NH_3 partial pressure ambient the contact resistivity became more uniform and decreased to about half.

The reason for ohmic contact formation with Ni was concluded to be the diffusion of Ga to Ni layer as seen in SR-XPS spectra, leading to Ga-vacancy induced levels close to valence band in the band gap. The diffusion and resulted degree of the crystallinity of formed Ga–Ni alloy is affected by the presence of NiO during heating: with NiO present, the formed alloy is more crystalline. This Ga-Ni interaction provides a previously not reported Ga 3d component, which can be used as a fingerprint. We expect that the Ga–Ni interface reaction increases the compensating N-vacancy formation, and therefore the post-heating environment has a significant effect on the contact resistivity, as found previously. Future studies can clarify a role of the crystalline Ga–Ni interface phase in the change of electrical properties from Schottky to ohmic behavior. For example, an epitaxial type of interface of GaNi/p-GaN might change the Schottky barrier height locally. Also, the effect of NH_3 background annealing to the interface composition requires more studying.

Acknowledgements

The authors thank the MAX IV and its staff for the possibility to conduct experiments at the FinEstBeams beam line. Financial support from Research Council of Finland and University of Turku Graduate School is acknowledged.

Conflict of Interest

The authors declare no conflict of interest.

Data Availability Statement

The data that support the findings of this study are available from the corresponding author upon reasonable request.

Keywords

p-GaN, Ni, SR-XPS

Received: February 20, 2025
Revised: May 15, 2025
Published online: June 12, 2025

[1] H. Amano, M. Kito, K. Hiramatsu, I. Akasaki, *Jpn. J. Appl. Phys.* **1989**, *28*, L2112.
[2] S. Nakamura, N. Iwasa, M. S. Masayuki Senoh, T. M. Takashi Mukai, *Jpn. J. Appl. Phys.* **1992**, *31*, 1258.
[3] G. Greco, F. Iucolano, F. Roccaforte, *Appl. Surf. Sci.* **2016**, *383*, 324.
[4] K. A. Rickert, A. B. Ellis, J. K. Kim, J.-L. Lee, F. J. Himpsel, F. Dwikusuma, T. F. Kuech, *J. Appl. Phys.* **2002**, *92*, 6671.
[5] Q. Z. Liu, S. S. Lau, *Solid-State Electron.* **1998**, *42*, 677.
[6] B. Monemar, P. P. Paskov, G. Pozina, C. Hemmingsson, J. P. Bergman, T. Kawashima, H. Amano, I. Akasaki, T. Paskova, S. Figge, D. Hommel, A. Usui, *Phys. Rev. Lett.* **2009**, *102*, 235501.
[7] P. Kozodoy, H. Xing, S. P. DenBaars, U. K. Mishra, A. Saxler, R. Perrin, S. Elhamri, W. C. Mitchel, *J. Appl. Phys.* **2000**, *87*, 1832.
[8] L.-C. Chen, J.-K. Ho, C.-S. Jong, C. C. Chiu, K.-K. Shih, F.-R. Chen, J.-J. Kai, L. Chang, *Appl. Phys. Lett.* **2000**, *76*, 3703.
[9] M. Christis, A. Henning, J. D. Bartl, A. Zeidler, B. Rieger, M. Stutzmann, I. D. Sharp, *Adv. Mater. Interfaces* **2024**, *11*, 2300758.
[10] D. Mistele, F. Fedler, H. Klausing, T. Rotter, J. Stemmer, O. Semchinova, J. Aderhold, *J. Cryst. Growth* **2001**, *230*, 564.
[11] H. W. Jang, S. Y. Kim, J.-L. Lee, *J. Appl. Phys.* **2003**, *94*, 1748.
[12] J. Smalc-Koziorowska, S. Grzanka, E. Litwin-Staszewska, R. Piotrzkowski, G. Nowak, M. Leszczynski, P. Perlin, E. Talik, J. Kozubowski, S. Krukowski, *Solid-State Electron.* **2010**, *54*, 701.
[13] D. Kim, S.-Y. Moon, S.-B. Bae, H.-T. Kwak, H. Park, H.-S. Lee, *Appl. Phys. Lett.* **2025**, *126*, 122108.
[14] C. Tang, C. Deng, C. Fu, J. He, F. Du, P. Wang, K. Wen, Y. Zhang, Y. Jiang, N. Tao, W. Yu, Q. Wang, H. Yu, *IEEE Electron Device Lett.* **2025**, *46*, 24.
[15] R. Pärna, R. Sankari, E. Kukk, E. Nõmmiste, M. Valden, M. Lastusaari, K. Kooser, K. Kokko, M. Hirsimäki, S. Urpelainen, P. Turunen, A. Kivimäki, V. Pankratov, L. Reisberg, F. Hennies, H. Tarawneh, R. Nyholm, M. Huttula, *Nucl. Instrum. Methods Phys. Res., Sect. A* **2017**, *859*, 83.

© 2025 The Author(s). Advanced Materials Interfaces published by Wiley-VCH GmbH

21967350, 2025, 13, Downloaded from https://advanced.onlinelibrary.wiley.com/doi/10.1002/admi.202500163 by Duodecim Medical Publications Ltd, Wiley Online Library on [27/08/2025]. See the Terms and Conditions (https://onlinelibrary.wiley.com/terms-and-conditions) on Wiley Online Library for rules of use; OA articles are governed by the applicable Creative Commons License

[16] K. Chernenko, A. Kivimäki, R. Pärna, W. Wang, R. Sankari, M. Leandersson, H. Tarawneh, V. Pankratov, M. Kook, E. Kukk, L. Reisberg, S. Urpelainen, T. Käämbre, F. Siewert, G. Gwalt, A. Sokolov, S. Lemke, S. Alimov, J. Knedel, O. Kutz, T. Seliger, M. Valden, M. Hirsimäki, M. Kirm, M. Huttula, *J. Synchrotron Radiat.* **2021**, *28*, 1620.
[17] D. K. Schroder, *Semiconductor Material and Device Characterization*, 1st edn., Wiley, **2005**.
[18] P. Laukkanen, M. P. J. Punkkinen, M. Kuzmin, K. Kokko, J. LÄng, R. M. Wallace, *Appl. Phys. Rev.* **2021**, *8*, 011309.
[19] J. Moudler, W. Stickle, P. Sobol, K. Bomben, *Handbook of X-ray Photoelectron Spectroscopy*, Perkin-Elmer Corporation, **1992**.
[20] J. Mäkelä, M. Tuominen, T. Nieminen, M. Yasir, M. Kuzmin, J. Dahl, M. Punkkinen, P. Laukkanen, K. Kokko, J. Osiecki, K. Schulte, M. Lastusaari, H. Huhtinen, P. Paturi, *J. Phys. Chem. C* **2016**, *120*, 28591.
[21] P. Laukkanen, M. Punkkinen, M. Kuzmin, K. Kokko, X. Liu, B. Radfar, V. Vähänissi, H. Savin, A. Tukiainen, T. Hakkarainen, J. Viheriälä, M. Guina, *Rep. Prog. Phys.* **2024**, *87*, 044501.
[22] J. Sun, K. A. Rickert, J. M. Redwing, A. B. Ellis, F. J. Himpsel, T. F. Kuech, *Appl. Phys. Lett.* **2000**, *76*, 415.
[23] G. Greco, P. Prystawko, M. Leszczyński, R. Lo Nigro, V. Raineri, F. Roccaforte, *J. Appl. Phys.* **2011**, *110*, 123703.
[24] J.-S. Jang, I.-S. Chang, H.-K. Kim, T.-Y. Seong, S. Lee, S.-J. Park, *Appl. Phys. Lett.* **1999**, *74*, 70.
[25] Y. Liu, *IOP Conf. Ser.: Mater. Sci. Eng.* **2020**, *738*, 012007.
[26] J.-L. Lee, M. Weber, J. K. Kim, J. W. Lee, Y. J. Park, T. Kim, K. Lynn, *Appl. Phys. Lett.* **1999**, *74*, 2289.
[27] M. Grodzicki, P. Mazur, S. Zuber, J. Pers, J. Brona, A. Ciszewski, *Appl. Surf. Sci.* **2014**, *304*, 24.
[28] S. Hautakangas, V. Ranki, I. Makkonen, M. Puska, K. Saarinen, L. Liszkay, D. Seghier, H. Gislason, J. Freitas, Jr, R. Henry, X. Xu, D. Look, *Phys. B* **2006**, *376-377*, 424.
[29] Z. Yang, L. K. Li, J. Alperin, W. I. Wang, *J. Electrochem. Soc.* **1997**, *144*, 3474.

© 2025 The Author(s). Advanced Materials Interfaces published by Wiley-VCH GmbH

21967350, 2025, 13, Downloaded from https://advanced.onlinelibrary.wiley.com/doi/10.1002/admi.202500163 by Duodecim Medical Publications Ltd, Wiley Online Library on [27/08/2025]. See the Terms and Conditions (https://onlinelibrary.wiley.com/terms-and-conditions) on Wiley Online Library for rules of use; OA articles are governed by the applicable Creative Commons License